Systems/Circuits

Effects of Locomotion on Visual Responses in the Mouse Superior Colliculus

Elise L. Savier,[1,2] Hui Chen,[1,2] and Jianhua Cang[1,2]
Departments of [1]Biology and [2]Psychology, University of Virginia, Charlottesville, Virginia 22904

Visual responses are extensively shaped by internal factors. This effect is drastic in the primary visual cortex (V1), where locomotion profoundly increases visually-evoked responses. Here we investigate whether a similar effect exists in another major visual structure, the superior colliculus (SC). By performing two-photon calcium imaging of head-fixed male and female mice running on a treadmill, we find that only a minority of neurons in the most superficial lamina of the SC display significant changes during locomotion. This modulation includes both increase and decrease in response amplitude and is similar between excitatory and inhibitory neurons. The overall change in the SC is small, whereas V1 responses almost double during locomotion. Additionally, SC neurons display lower response variability and less spontaneous activity than V1 neurons. Together, these experiments indicate that locomotion-dependent modulation is not a widespread phenomenon in the early visual system and that the SC and V1 use different strategies to encode visual information.

Key words: behavioral state; direction selectivity; locomotion; superior colliculus; two-photon imaging; visual cortex

Significance Statement

Visual information captured by the retina is processed in parallel through two major pathways, one reaching the primary visual cortex through the thalamus, and the other projecting to the superior colliculus. The two pathways then merge in the higher areas of the visual cortex. Recent studies have shown that behavioral state such as locomotion is an essential component of vision and can strongly affect visual responses in the thalamocortical pathway. Here we demonstrate that neurons in the mouse superior colliculus and primary visual cortex display striking differences in their modulation by locomotion, as well as in response variability and spontaneous activity. Our results reveal an important "division of labor" in visual processing between these two evolutionarily distinct structures.

Introduction

Seeing is an active process that is highly dependent on our intention, expectation, and behavioral state. In mammals, visual information captured by the retina is processed in parallel through two major pathways, one reaching the primary visual cortex (V1) through the thalamus, and the other projecting to the superior colliculus (SC). Neurons in these visual structures encode information by responding to specific features of the stimulus in their receptive fields (Kuffler, 1953; Hubel and Wiesel, 1962). The activity of these visual neurons is also modulated by nonvisual inputs, such as attention, arousal, and locomotor activity (Livingstone and Hubel, 1981; Steriade et al., 2001; Maunsell, 2015; Busse et al., 2017), presumably mediating visual behaviors in a context-dependent manner. Recent studies in mice have shown that such a modulation occurs early along the visual pathways. For example, V1 neurons dramatically increase their visually-evoked responses when the mouse is running (Niell and Stryker, 2010), and this locomotion-dependent modulation is largely limited to layer 2/3 excitatory cells in adult mice (Niell and Stryker, 2010; Hoy and Niell, 2015).

Following the original finding by Niell and Stryker (2010), numerous studies have characterized the state-dependent modulation of V1 responses and examined the underlying cortical and subcortical circuits (Ayaz et al., 2013; Bennett et al., 2013; Polack et al., 2013; Saleem et al., 2013; Fu et al., 2014; Lee et al., 2014; Vinck et al., 2015; Mineault et al., 2016; Pakan et al., 2016; Dadarlat and Stryker, 2017; Dipoppa et al., 2018). Others have shown that the locomotion-dependent response increase can be observed as early as in the visual thalamus (Erisken et al., 2014; Aydın et al., 2018). Together, these studies highlight the notion that behavioral state such as locomotion is an essential component of vision and can strongly affect visual responses in the thalamocortical pathway.

Received July 31, 2019; revised Sept. 3, 2019; accepted Sept. 24, 2019.

Author contributions: E.L.S. and J.C. designed research; E.L.S. performed research; E.L.S., H.C., and J.C. analyzed data; E.L.S. and J.C. wrote the paper.

This work was supported by U.S. National Institutes of Health Grants (EY026286 and EY020950) to J.C. We thank Dr. Na Ji and Dr. Wenzhi Sun for help with developing the surgical procedure to expose the SC, Dr. Rolf Skyberg and James Cole for comments on the paper, and the Jefferson Scholars Foundation for financial support.

The authors declare no competing financial interests.

Correspondence should be addressed to Jianhua Cang at cang@virginia.edu.

https://doi.org/10.1523/JNEUROSCI.1854-19.2019

Copyright © 2019 the authors

The SC is the other major visual center that is evolutionarily conserved in all vertebrates. This midbrain structure is layered, with its superficial layers being visual and deeper layers multimodal and premotor (May, 2006; Cang and Feldheim, 2013). The most superficial cellular layer of the SC is the stratum griseum superficiale (SGS), which receives direct retinal input from ganglion cell axons that course through the deeper stratum opticum (May, 2006). In mice, >85% of retinal ganglion cells project to the SC (Ellis et al., 2016), making it the most prominent visual processing center in this species (Cang et al., 2018). Recent studies have revealed more diverse visual response properties in the mouse SGS than in primates, including selectivity for movement direction and stimulus orientation (Wang et al., 2010; Gale and Murphy, 2014; Ahmadlou and Heimel, 2015; Inayat et al., 2015; Ito et al., 2017; De Franceschi and Solomon, 2018). In particular, the most superficial lamina of the SGS (sSGS) is enriched with highly direction-selective neurons that are specialized in encoding visual motion (Inayat et al., 2015; Barchini et al., 2018). Given the SC's prominent role in mouse visual behaviors and especially in motion processing, we investigate in this study whether neurons in the sSGS also display locomotion-dependent modulation.

By performing two-photon calcium imaging in head-fixed mice running freely on a treadmill, we find that only a small fraction (~30%) of sSGS neurons display a significant modulation during locomotion. This modulation does not follow a particular trend (increase or decrease) in visual responses and is small in magnitude (~10% overall increase). We then image V1 under the same condition and found that its responses almost double during locomotion. Furthermore, our imaging experiments reveal that SC neurons show lower response variability and fewer spontaneous events than V1 neurons. Together, these experiments reveal an important "division of labor" in visual processing between these two evolutionarily distinct structures, in which the sSGS provides a faithful encoding of visual information independent of behavioral state, whereas V1 may contribute to response flexibility under different behavioral contexts by integrating nonvisual inputs.

Materials and Methods

Animals. Adult C57BL/6 mice of either sex were used in this study, including both wild-type ($n = 12$, 2–6 month old) and transgenic mice to express the red fluorescent protein tdTomato in glutamate decarboxylase two positive ($GAD2^+$, GABAergic) neurons ($n = 8$, 6 for SC imaging, 2 for V1 imaging, 2–4 month old). The transgenic mice were obtained by crossing *Gad2*-IRES-cre mice (The Jackson Laboratory, Stock #010802; RRID:IMSR_JAX:010802) with an Ai9 line (*RCL-tdT*, Stock #007909; RRID:IMSR_JAX:007909) in our colony. All mice were kept on a 12 h light/dark cycle, with two to five animals housed per cage. Whenever possible, social housing was maintained after surgery and animals were kept for up to 3 months. All experimental procedures were approved by the University of Virginia Institutional Animal Care and Use Committee.

Surgery: SC. Mice were anesthetized with isoflurane (4% for induction, 2% for maintenance, in O_2, ~0.5 L/min; VetFlo, Kent scientific). Once the animals lost reflexes, the scalp was shaved and lidocaine applied on the ear bars, before placing the animals in a stereotaxic frame (Digital Model 1900, Stereotaxic Alignment System, Kopf Instruments). Body temperature was maintained with a heating pad equipped with a feedback heater control module monitored via a rectal thermoprobe (Frederick Haer). Artificial tears (Henry Schein) were applied to the eyes for protection during surgery. Skin was disinfected using alternating scrubs of 70% ethanol and betadine and removed to expose the skull. The skull was scraped to remove connective tissue and to allow adherence later in the procedure.

A ~2.5 mm craniotomy was performed over lambda using a dental drill and a ¼ RA drill bit (Model XL-230, Osada, and Midwest Dental Equipment, respectively). The skull was thinned and soaked in sterile saline solution. This eased the separation of the bone from the dura along the sutures before removal. Gelfoam (Pfizer Injectables) soaked in saline was used throughout the procedure to stop any bleeding and to maintain osmosis once the brain was exposed. The dura, which is thick above the SC, was opened using a 30 G needle and torn along the latero-medial axis, thus revealing the caudal pole of the SC.

Once the SC was exposed, AAV1-Syn-GCaMP6f viral vector (RRID: Addgene_100837; pAAV.Syn.GCaMP6f.WPRE.SV40, 1:1 in PBS, titer 2×10^{13}) was injected using a Nanoject II (Drummond Scientific) fitted with a glass pipette with a beveled tip. Pipette was loaded with the viral vector and coordinates were zeroed on the SC surface. The pipette was lowered into the SC down to 500 μm, and then retracted back to two injections sites at 400 and 200 μm below surface, respectively. At each depth, a total volume of ~50 nl was delivered, in 2.3 nl pulses, 15 s apart. The pipette was left in the tissue for 5 min before being slowly retracted. Once injections were done, a glass window was placed into the craniotomy. The windows consisted in 4 pieces of #1.5 glass coverslips, custom cut by Potomac Laser, glued together with UV glue (Norland Optical Adhesives). From top to bottom, the four pieces are a ring-shaped piece (inner diameter: 2.2 mm, outer diameter: 4.2 mm), a disk (∅2.5 mm) and two equilateral triangles (2 mm). The triangle shape allowed to catch the dura and drag it anteriorly, pushing forward the transversal sinus. Once in place, windows were pushed down and sealed with VetBond (3M). A head bar was finally mounted on the skull using Metabond (Parkell) mixed with black ink to avoid reflections during imaging.

Mice were given a dose of carprofen (5 mg/Kg; Sub-Q) and 0.5 ml of sterile saline (Sub-Q) toward the end of the surgery. Animals were placed in a heated chamber until ambulatory and then transferred back to their home cage. They were monitored daily for pain and wound health. Imaging was performed ~3 weeks after injection.

Surgery: V1. A similar procedure was used for implementing chronic cranial windows over V1. In this case, windows consisted of only two pieces of glass coverslips, the ring and the disk. Craniotomy was performed 2.75 mm lateral from the midline and along the lambdoid suture. The same amount of AAV1-Syn-GCaMP6f viral vector was injected at a depth of 500 and 250 μm, at three different locations, 500 μm apart, around the center of the craniotomy.

Two-photon calcium imaging. After the mice had fully recovered, they were habituated to head-fixation and running on the cylindrical treadmill. Once animals were comfortable with the setup, imaging was performed under a two-photon scanning microscope (Ultima Investigator, Bruker Nano Surface Division; RRID:SCR_017142). A ring was added on top of the head-plate to hold water for immersion of the objective and surrounded by a shield to block light originating from the visual stimulus during imaging. Imaging was performed with a Ti:sapphire laser (Chameleon Discovery with TPC, Coherent) at excitation wavelength of 920 nm for GCaMP6f using a 16× 0.8 NA Nikon objective. Emitted signals from GCaMP6f and tdTomato were filtered into separate PMTs (green and red channels).

Imaging data were acquired using the PrairieView software v5.4 with a resonant scanner at 2× optical zoom, resulting in a 412.2 × 412.2 μm field-of-view. Image resolution was 512 × 512 pixels and the acquisition rate was 30 Hz. Frame-averaged data were used for the analysis (4-frame averages). Imaging was performed in the sSGS (no deeper than 50 μm from the SC surface). For V1 imaging, data were acquired with the same parameters at a depth of ~150 μm.

Note that animals that had sustained pia inflammation or in which there was poor expression of GCaMP6f were not subject to imaging.

Visual stimulus. Visual stimuli were generated with MATLAB Psychophysics toolbox (Brainard, 1997; Niell and Stryker, 2008; RRID: SCR_002881) on an LCD monitor (37.5 × 30 cm, 60 Hz refresh rate, ~50 cd/m^2 mean luminance, gamma corrected). The screen was placed 25 cm away from the eye contralateral to the imaging site (the right eye). The monitor was moved for every imaged field-of-view so that the cells' receptive fields were near the center of the screen. The placement of the monitor center in visual space varied between 30° and 60° in elevation

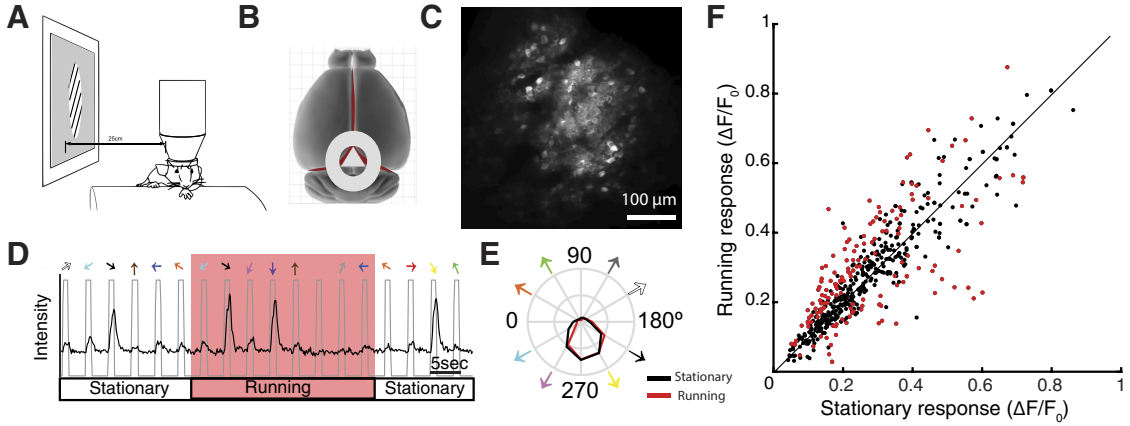

Figure 1. Minor effect of locomotion on visual responses in the sSGS. ***A***, Schematic of the imaging setup. Stimulus monitor was placed at the retinotopic location corresponding to the imaged area while mice were running freely on a cylindrical treadmill. ***B***, Schematic of the position of the cranial window, which reveals caudal-medial portion of the SC while preserving the cortex. ***C***, An example image of the field-of-view during two-photon imaging. Neurons were expressing GCaMP6f via AAV transfection. Scale bar, 100 μm. ***D***, Raw calcium trace of an imaged neuron during presentation of visual stimuli (drifting gratings, 12 directions). The gray line marks the period of visual stimulation, with colored arrows on top indicating the direction of the presented gratings. The red shaded region indicates the period when the mouse was running. ***E***, Direction tuning curves of the example cell, plotting the mean $\Delta F/F_0$ at each stimulus direction, averaged over multiple repeats per direction. Black, Stationary; red, running. ***F***, Comparison of SC neurons' responses between running and stationary conditions. Each dot is the averaged responses of an individual neuron, with red dots marking those that were statistically different between running and stationary conditions ($n = 157$ of total 528 cells; 29.7%; $n = 12$ mice; Wilcoxon signed rank test). The black line indicates the line of equality to facilitate comparison.

(0° representing eye-level) and between 90° and 120° across the azimuth (0° representing the center of the binocular field) in all imaging experiments reported in this study.

The visual stimulus was a sinusoidal wave drifting gratings (100% contrast, 0.08 cpd, 2 Hz), presented on a gray background in a circular patch (40° diameter) at the center of the screen. To assess responses to motion direction, 12 different directions were used, ranging from 0° to 330° and tiling all direction space in 30° increments. Zero degree represented forward motion from the animal's perspective. A blank (gray) condition was added to the 12 directions. Each stimulus condition of the gratings was presented for 1 s, followed by a gray screen for 3 s. The entire stimulus set was shown to the mouse at least 10 times in a pseudorandom fashion for every imaged field-of-view. For V1 imaging, full screen sinusoidal drifting grating of 12 directions (similar to SC) were presented in a pseudo-randomized fashion (1 s stimuli, 3 s wait interval, 2 Hz, 0.08 cpd).

The timing and parameters of each presented visual stimulus were recorded by the PrairieView software simultaneously with the imaging data. Onset and offset of the visual stimulus were recorded in a third channel (in addition to red and green) to ensure synchronization of the events, and stimulus conditions were encoded in voltage signals. The rotation of the treadmill (i.e., the locomotion of the mouse) was recorded via a rotary encoder generating transistor-transistor logic pulses (100 pulses/revolution), which were used to estimate the speed of the animal.

Imaging data analysis. Time-series frames were used to produce an average image of the field-of-view to identify cell bodies. In the cases where the imaging field shifted in the *x-y* plane over the course of the series, an automated procedure was used to realign the frames. To determine whether each selected region-of-interest (ROI) is an inhibitory ($GAD2^+$) or excitatory neuron ($GAD2^-$), the experimenter referred to the red channel image of each field-of-view where $GAD2^+$ cells were labeled with tdTomato. This selection process relied exclusively on the expression of tdTomato and was performed blindly to the functional properties of the cells, which were determined at a later stage of the process. Note that cells that displayed a high level of correlation between the red and the green channels were excluded for this analysis, because this fluctuation in signal was due to motion artifact.

For the analysis of calcium imaging data, we followed our published procedures (Inayat et al., 2015; Levine et al., 2017; Barchini et al., 2018). Briefly, ROIs were manually drawn on the average image of the collected time-series, and the intensity values of all pixels in each ROI were averaged for each frame to obtain the raw Ca^{2+} signal. From the raw trace, and for each stimulus presentation, $\Delta F/F_0 = (F - F_0)/F_0$, was calculated, where F_0 was the mean of the baseline signal over a fixed number of frames (6) before stimulus onset and F was the average fluorescence signal over 8 frames, 1 frame after stimulus onset. A cell was considered responsive if its mean $\Delta F/F_0$ was >2 SD above its F_0 for at least one of the stimulus conditions. The mean value of $\Delta F/F_0$ for each of the stimulus conditions was then used for subsequent data analysis for all the responsive cells. Note that in our previous imaging studies of the mouse SGS (Inayat et al., 2015; Barchini et al., 2018), we compared calcium signals and spiking activity by simultaneous two-photon imaging and cell-attached recording. Those experiments revealed a linear correlation between the two measures that is similar to what was observed in cortical imaging (Chen et al., 2013), thus indicating that two-photon imaging can be reliably applied to the SGS.

Running and stationary conditions were defined as follow: if the speed of the animal was >1 cm/s both prior (0.75 s) and during the stimulus duration (1 s), the animal was considered running. If the speed of the animal was below this speed for both periods, the animal was considered stationary. Trials where both conditions were not fulfilled were excluded.

To quantify the degree of direction selectivity, we calculated a global direction selectivity index (gDSI), which is the vector sum of $\Delta F/F_0$ responses normalized by their scalar sum (Gale and Murphy, 2014; Inayat et al., 2015): $\text{gDSI} = \frac{\sum R_\theta e^{i\theta}}{\sum R_\theta}$, where R_θ is the response magnitude in $\Delta F/F_0$ at direction θ of the stimulus. To determine the locomotion-dependent modulation of the responses and tuning of sSGS neurons (Figs. 1–4), we excluded imaging sessions where not all 12 stimulus directions were encountered during both stationary and running conditions.

To determine the effect of locomotion, we calculated a locomotion modulation index (LMI) as follow: $LMI = \frac{R_{running} - R_{stationary}}{R_{running} + R_{stationary}}$, where R_{running} is the averaged response during running condition and $R_{\text{stationary}}$ is the response during stationary condition. For Figures 1–4, the index was calculated using the average response of the entire tuning curve. For Figure 5*C*, the index was calculated using the mean response to each stimulus direction.

For the analysis of trial-to-trial variability, we analyzed the responses at the preferred direction, by calculating the Fano factor $F = \frac{\sigma^2}{\mu}$ (i.e., the variance of the response magnitudes over all trials divided by the mean).

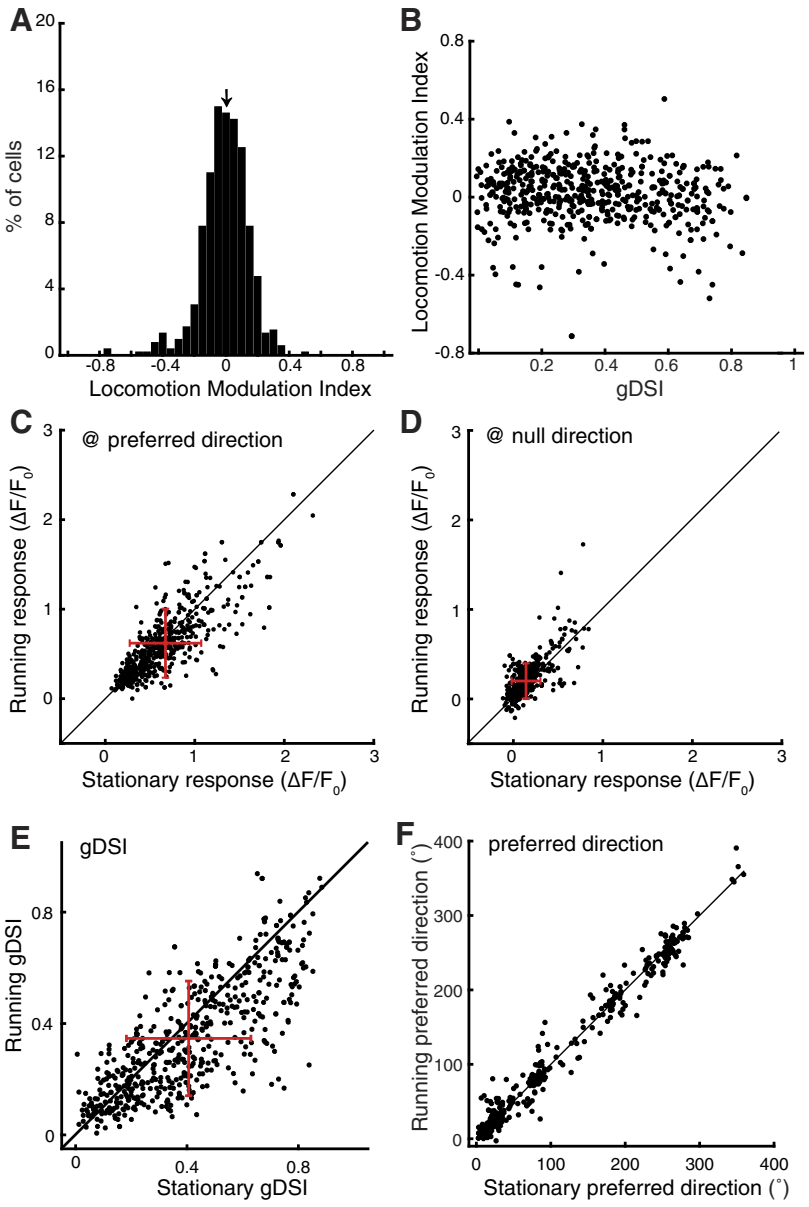

Figure 2. Quantification of the effect of locomotion on visual responses in the sSGS. ***A***, A histogram of LMI for average responses over the entire tuning curve. The arrow on top of the histogram marks the median value of the distribution (median of LMI = 0.03; $n = 528$ cells). ***B***, A plot of LMI against gDSI for these cells. ***C***, Comparison of SC neurons' responses at their preferred stimulus direction between running and stationary conditions. ***D***, The same plot for responses at the direction opposite to the preferred direction ("null" direction). ***E***, Comparison of gDSI for individual neurons during running and stationary conditions. ***F***, Comparison of the preferred direction for direction selective cells (gDSI > 0.25 combining both running and stationary conditions). The black lines in ***C***–***F*** indicate the line of equality; the red crosses in ***C***–***E*** indicate the mean and SD of dataset; $n = 528$ from 12 mice for ***A***–***E***, $n = 360$ (gDSI > 0.25) for ***F***.

Only conditions with a minimum of three trials were included in this analysis, resulting in the exclusion of two V1 cells for running condition.

For the quantification of spontaneous events, calcium signals were recorded for 10 min in either complete darkness or with a gray screen at the previously recorded location. Raw calcium traces were smoothed over 15 frames (0.5 s). The baseline of each trace was the value that had the highest occurrence across the recording period. Twice the value of the baseline was used as a threshold to detect the occurrence of a spontaneous event.

Statistics. Significance was calculated using two-sided statistical tests including Kolmogorov–Smirnov (KS) tests and Wilcoxon signed rank tests as stated. All analyses and graph plotting were performed in MATLAB (MathWorks; RRID:SCR_001622). No statistical methods were used to predetermine sample sizes, but our sample sizes are similar to those reported in the field. We did not randomly assign animals to groups because it is not applicable to the experimental design of this study.

Results

To determine whether neurons in the SC are subject to modulation during locomotion, we performed two-photon calcium imaging in awake mice. Animals were head-fixed under the microscope, able to run freely on a cylindrical treadmill (Fig. 1*A*). To gain optical access to the SC, we adapted a published procedure (Feinberg and Meister, 2015) to implant an imaging window at the caudal pole of the SC (see Materials and Methods; Fig. 1*B*). During the same surgery, viral vectors (AAV1) carrying genetically encoded calcium indicators (GCaMP6f) were injected into the SC. After 2–3 weeks of recovery, mice were habituated to head-fixation. Imaging was performed once the animal was comfortable with running on the treadmill. We were able to image visually-evoked responses of ~15% of the SC surface at cellular resolution (typical field-of-view shown in Fig. 1*C*) while preserving the entire cortex. This type of window allowed stable chronic imaging for up to 60 d (data not shown). In this study, we limited the imaging depth to ~50 μm below the SC surface, because large neuropil signals in deeper SGS render reliable determination of neuronal responses extremely difficult. We previously showed in anesthetized mice that most neurons in this lamina (sSGS) are direction selective (Inayat et al., 2015). This new preparation allowed us to study these neurons in awake condition, and more importantly, assess whether their responses are modulated by locomotion.

Minor effect of locomotion on visual responses in the sSGS

During imaging, visual stimuli were presented on an LCD monitor, placed 25 cm away from the mouse and centered to the responsive visual field. The stimuli consisted of a small patch (40° in diameter) of sinusoidal gratings drifting along 12 different directions (30° step between 0° and 360°, presented in random sequences). Consistent with previous results in anesthetized mice with cortex removed (Inayat et al., 2015; Shi et al., 2017; Barchini et al., 2018), most neurons in the sSGS were direction selective (Fig. 1*D*). Over the population, 69% cells ($n = 360/528$ cells from 12 mice) had a gDSI (see Materials and Methods for details of calculation) >0.25, indicating their high direction selectivity.

We next sorted the imaging trials according to the animal's locomotion. If the mouse was moving at a velocity >1 cm/s both

prior (0.75 s) and for the duration (1 s) of a particular stimulus, that trial was classified as a running condition; if the velocity was <1 cm/s for both time periods, the trial was considered stationary. The tuning curves of individual neurons were obtained separately for the two conditions (Fig. 1*E*). We calculated the mean of each tuning curve and used it to compare responses between running and stationary conditions (Fig. 1*F*). Overall, no prominent trend (i.e., increase or decrease) of locomotion-dependent modulation was seen for the whole population of sSGS neurons, unlike what has been reported for V1. We then compared the running and stationary tuning curves for individual neurons using paired comparisons, and a statistically significant change in response magnitude was found for 29.7% of the population (n = 157/528 cells; Wilcoxon signed ranked test, $p < 0.05$; Fig. 1*F*, red dots). Of these, 103 cells (19.5%) displayed increased responses and 54 (10.2%) displayed a decrease during running.

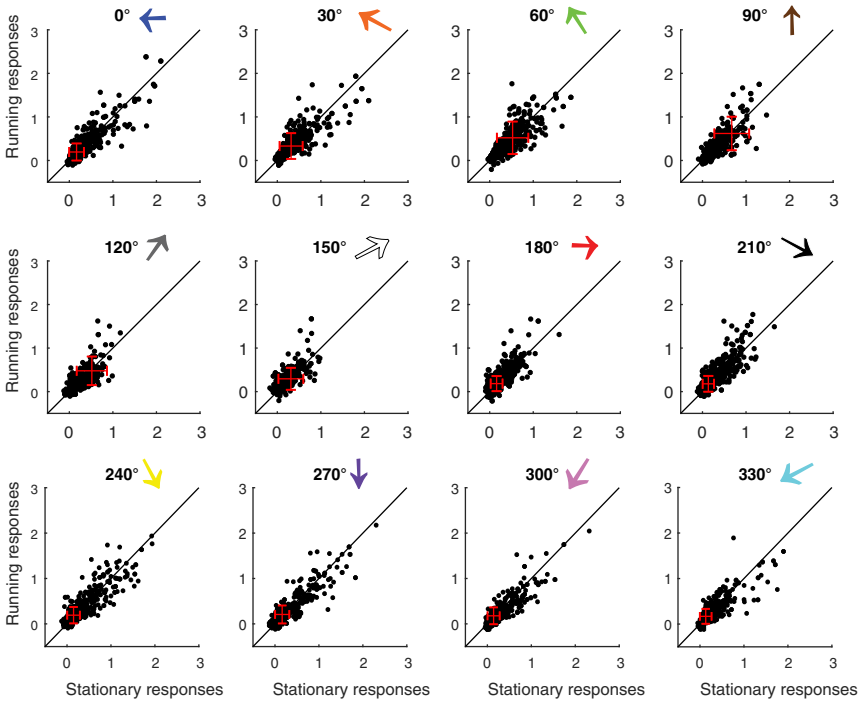

Figure 3. Comparison of sSGS neurons' responses to each stimulus direction between running and stationary conditions. Each panel plots neurons' responses to a particular stimulus direction under running and stationary conditions. The numbers and colored arrows on top of each plot indicate the stimulus direction, following the same convention as in Figure 1. The black lines indicate the line of equality to help comparison, and the red crosses indicate the mean and SD of each dataset.

We note that although the paired comparison of the two tuning curves is useful in determining an overall change in responsiveness for individual neurons, it could potentially mask more specific modulations. This is especially relevant given that the majority of sSGS neurons are direction selective, meaning that response magnitude is low to many stimulus directions. We thus performed three additional analyses to further characterize how locomotion might modulate sSGS responses and direction selectivity.

First, we calculated a LMI to quantify the effect of locomotion for each cell: $LMI = \frac{R_{running} - R_{stationary}}{R_{running} + R_{stationary}}$, (Pakan et al., 2016). Using the average of the tuning curves, the LMI of sSGS neurons was distributed ~0, with a median of 0.03 (Fig. 2*A*). Importantly, no correlation was found between this index and the gDSI of individual neurons (Fig. 2*B*), indicating that the effect of locomotion, which appears minor in the sSGS, does not depend on direction selectivity.

Second, we determined whether locomotion modulated sSGS responses differently at their preferred and non-preferred directions. At the preferred direction (which is different for each individual neuron), locomotion caused a slight, but statistically significant, reduction of the visual responses over the population (p = 3.56e-7, Wilcoxon test; Fig. 2*C*). In contrast, the responses to the direction opposite to the preferred ones were slightly increased during running (p = 1.16e-16, Wilcoxon test; Fig. 2*D*). Together, these changes led to a significant decrease of the gDSI under running condition across the population (p = 1.37e-19, Wilcoxon test; Fig. 2*E*). Nevertheless, the changes in response magnitude were small, such that the sSGS neurons maintained their direction preference between stationary and running conditions (Fig. 2*F*; p = 0.41, Wilcoxon test).

Finally, we determined whether locomotion modulation could depend on the specific direction of the visual stimulus. For example, a posteriorly moving stimulus is along the direction of the optic flow (180° by our convention), and could potentially be encoded differently in the SC than other directions during locomotion. We thus compared running and stationary responses of individual neurons separately for each of the 12 stimulus directions (Fig. 3). No apparent direction-specific trend of increase or decrease was seen, indicating that under our experimental condition, the minor modulation induced by locomotion does not depend on the direction of the visual stimulus.

Locomotion affects excitatory and inhibitory neurons similarly in the sSGS

Previous studies demonstrated that locomotion increases the responses of V1 excitatory neurons via a disinhibitory circuit (Fu et al., 2014; Lee et al., 2014). In other words, excitatory and inhibitory cells are differentially modulated by locomotion in V1. Inhibitory cells occupy a larger proportion in the SGS than in V1, accounting for ~30% of the population (Whyland et al., 2019). Consequently, a differential modulation of these two cell types, if it indeed exists in the SGS, could potentially explain the lack of consistent changes during running (i.e., increase vs decrease). We tested this possibility by performing the same imaging experiments in GAD2-cre mice crossed with a reporter strain (Ai9), so that inhibitory cells could be identified by the expression of tdTomato. As shown in Figure 4*A*, excitatory (GAD2$^-$) and inhibitory (GAD2$^+$) neurons could be differentiated by examining the overlap between red (tdTomato) and green fluorescent signals (GCaMP6f). We then compared the responses of the identified cells in stationary and running conditions, and found that the trend of modulation did not correlate with the identity of the cells (Fig. 4*B*). The LMI of the two functional cell types were similarly small (for GAD2$^-$: n = 51, median = 0.033, for GAD2$^+$; n = 42, median = −0.008, p = 0.506, KS test; from 6 mice; Fig. 4*C*). Overall, these experiments did not reveal a trend in the modula-

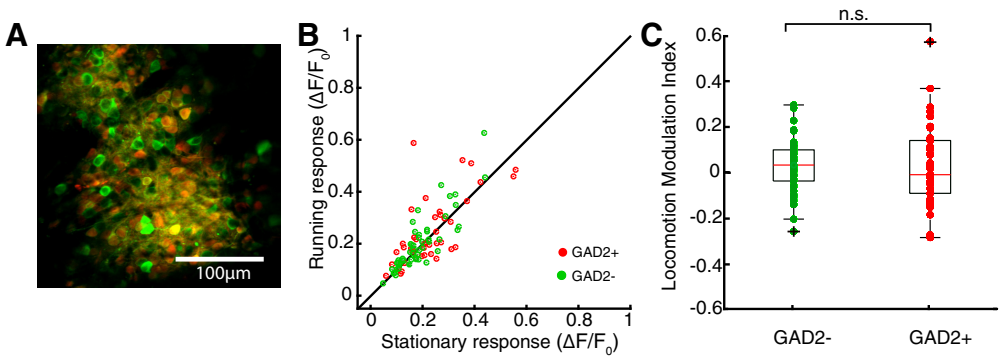

Figure 4. Minor effect of locomotion on both excitatory and inhibitory cells in the SC. ***A***, An example field-of-view of a mouse expressing tdTomato in Gad2 $^{+}$ cells. The image combines both red (i.e., tdTomato) and green (i.e., GCaMP6f) signals, allowing the identification of Gad2 $^{+}$ and Gad2 $^{-}$ cells under two-photon imaging. ***B***, Comparison of responses between running and stationary conditions for the two cell types. Red, Gad2 $^{+}$; green, Gad2 $^{-}$. ***C***, Locomotion modulation index for Gad2 $^{-}$ and Gad2 $^{+}$ cells. Individual data points are overlaid on the box-whisker plots. On each box, the central mark indicates the median, and the bottom and top edges of the box indicate the 25th and 75th percentiles, respectively. The whiskers extend to the most extreme data points not considered outliers, and the outliers are plotted individually using the + symbol. No statistically significant difference was seen between Gad2 $^{-}$ and Gad2 $^{+}$ cells ($p = 0.506$; $n = 51$ Gad2 $^{-}$; $n = 42$ Gad2 $^{+}$ cells; KS test; from 6 mice).

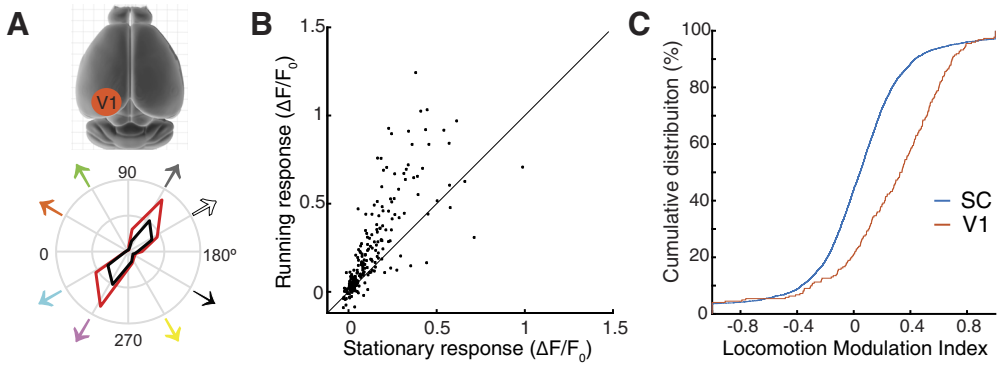

Figure 5. Locomotion modulates V1 and SC responses differently. ***A***, ***B***, Two-photon imaging of V1 confirms that cortical responses increase with locomotion. An example tuning curve of a V1 neuron is shown in ***A*** (bottom). Black, Stationary; red, running. ***B***, The response amplitude of V1 neurons to all stimulus directions are shown to compare running and stationary conditions. ***C***, Cumulative distribution of locomotion modulation index for V1 and SC responses (V1: $n = 20$ cells, 240 stimulus conditions; SC: $n = 528$ cells, 6336 conditions; $p = 2.98\text{e-}24$, KS test).

tion as a function of cell type, suggesting different effects of locomotion in the SC and V1.

Locomotion has different effects in V1 and SC

The surprisingly subtle effect of locomotion on sSGS neuronal responses led us to conduct imaging experiments on V1 using the same setup, allowing us to directly compare those two visual structures. Consistent with previous studies, layer 2/3 neurons in V1 displayed a robust increase in response amplitude during locomotion (Fig. 5*A*,*B*). Using the same index (LMI) as used in the SC, we quantified the effect of locomotion on V1 neurons' responses to all stimulus directions. The LMI distribution was skewed toward positive values for V1 cells, with a median value of 0.29 ($n = 20$ cells, and 240 conditions; Fig. 5*C*). This value of LMI indicates an almost twofold (182%) increase of visual responses under running condition, similar to what has been reported for V1 layer 2/3 cells (Hoy and Niell, 2015). In contrast, in the sSGS, the LMI of responses to all stimulus conditions were near 0, with a median of 0.05 (corresponding to ~10% increase; $n = 528$ cells, and 6336 conditions), significantly smaller than in V1 ($p = 2.98\text{e-}24$, KS test; Fig. 5*C*). These results thus highlight the dramatic difference in how locomotion affects the encoding of visual motion throughout the early visual system.

In addition to modulation by locomotion, our imaging experiments also revealed two other differences between V1 and the SC, namely, response variability and spontaneous activity. First, to examine trial-to-trial variability, we compared the responses of collicular and cortical neurons to the repeated presentation of the same stimulus at their preferred directions. In the sSGS, the same stimulus elicited strong and consistent responses (Fig. 6*A*,*B*), whereas more variable responses were observed for V1 neurons (Fig. 6*D*,*E*). We quantified this observation by calculating the Fano factor (variance/mean of the response magnitudes; Kara et al., 2000; Sarnaik et al., 2014) for V1 and sSGS neurons (Fig. 6*G*). The Fano factor was much greater (i.e., more variable responses) for V1 neurons (median = 0.03 for SC, stationary and running combined, median = 0.13 for V1, $p = 3.5\text{e-}8$ between SC and V1 under stationary condition, $p = 0.027$ for running condition, KS test).

Next, to examine spontaneous activity, we imaged neuronal populations in V1 layer 2/3 and the sSGS for a period of 10 min in either complete darkness or with a gray screen. We calculated a threshold of event detection for each recording (twofold of the baseline; see Materials and Methods) to quantify the number of spontaneous events. In the sSGS, very few of these events can be observed, both in total darkness and with a gray screen (Fig. 6*C*). In fact, many sSGS neurons were completely inactive during the entire 10 min sessions ($n = 22/50$ cells in dark and 30/50 in gray; Fig. 6*H*). In contrast, V1 neurons showed a much greater number of spontaneous events (median = 2, mean = 6.0 ± 5.5 for V1, $n = 56$; median = 0, mean = 1.5 ± 0.8 for SC, $n = 50$; Fig. 6*H*;

$p = 0.0049$ for dark condition between SC and V1 and $p = 6.35e\text{-}4$ for gray condition, KS test).

Overall, these results demonstrate that V1 neurons display a higher amount of spontaneous activity than sSGS neurons, which might contribute to the larger response variability in V1. These observations, together with the finding of a much smaller locomotion-dependent modulation in the sSGS, are consistent with the notion that sSGS neurons provide a more faithful encoding of visual stimulation independent of internal state, whereas V1 neurons may contribute to response flexibility under different behavioral contexts via their nonvisual inputs.

Discussion

Visual processing in the SC and locomotion-dependent modulation

In this study, we have demonstrated that visual neurons in the SC and V1 display striking differences in their modulation by locomotion, response variability, and spontaneous activity. These results highlight the distinct roles that the two structures play in visual processing. The visual cortex is involved in perception, and has been shown to be modulated by many nonvisual factors. For example, activities in rodent V1 can be shaped by reward timing (Shuler and Bear, 2006), locomotion (Niell and Stryker, 2010), arousal (Reimer et al., 2014; Vinck et al., 2015), auditory input (Iurilli et al., 2012; Ibrahim et al., 2016), sensorimotor mismatch (Keller et al., 2012; Roth et al., 2016), and perceptual learning (Poort et al., 2015). On the other hand, the SC is associated with the detection of abrupt change, such as light flashes and motion, to generate orienting or escaping responses (Zhao et al., 2014; Liang et al., 2015; Shang et al., 2015; Wei et al., 2015; Zingg et al., 2017). With their lower spontaneous activity and response variability, as well as the weak modulation by locomotion, sSGS neurons in the SC are positioned to faithfully encode visual information to generate reliable behavioral response. Our study thus provides novel insights into the function and organization of the mammalian visual system.

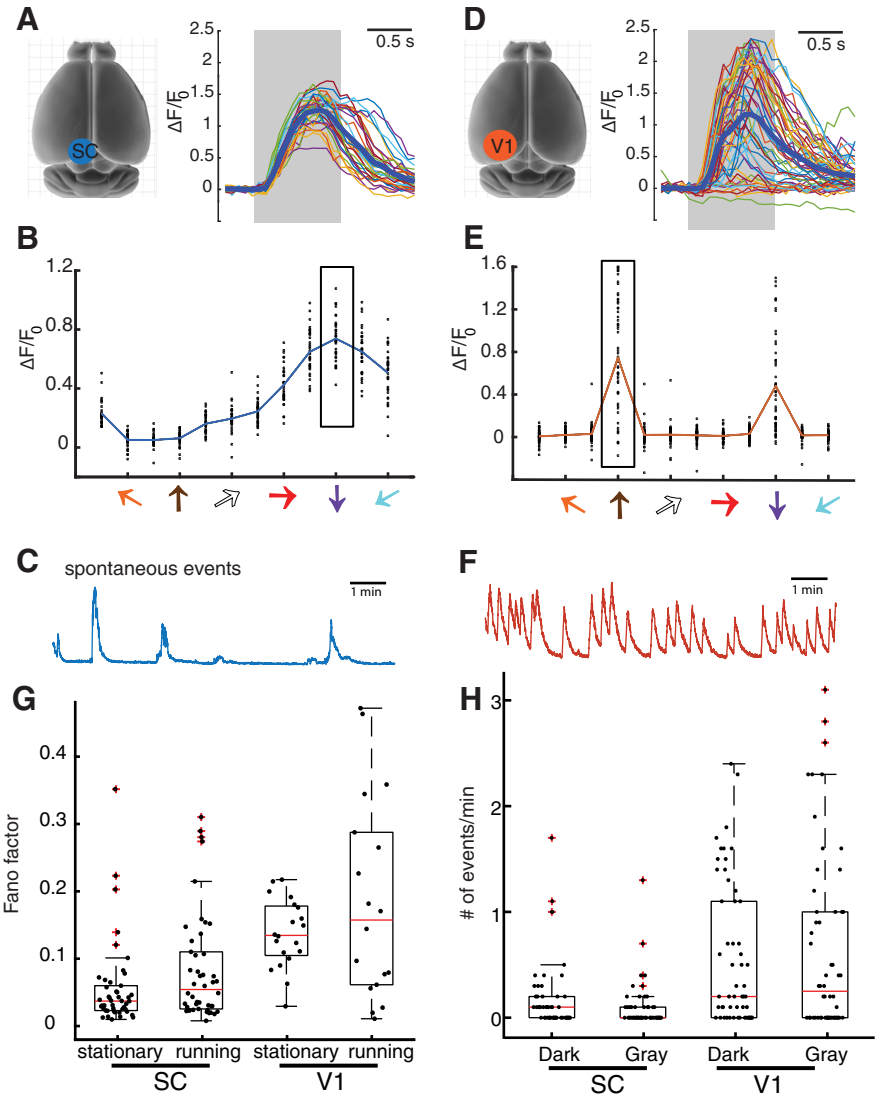

Figure 6. sSGS neurons have less response variability and fewer spontaneous events than V1 neurons. ***A***, Calcium transients of an example sSGS neuron in response to gratings drifting at its preferred direction. The gray region marks the duration of the visual stimulus. A total of 33 repeats were overlaid in thin color lines, and the average is shown in the thick blue line. ***B***, Direction tuning curves of the example neuron. The scattered dots at each direction are responses of individual repeats, and the rectangle box marks the responses at the preferred direction, corresponding to the traces in ***A***. ***C***, An example trace of spontaneous calcium events of a SC neuron. ***D–F***, Similar plots as in ***A–C*** for V1 neurons. ***G***, Quantification of response variability of SC and V1 neurons at the preferred directions. V1 neurons show significantly higher Fano factor compared with SC neurons (V1: $n = 20$ cells for stationary and 18 for running; SC: $n = 46$ cells for stationary and 46 for running; $p = 3.5e\text{-}8$ between V1 and SC under stationary condition, $p = 0.027$ for running condition, KS test). ***G***, Quantification of spontaneous activity of SC and V1 neurons under uniform dark or gray screen. V1 neurons had significantly more spontaneous events than SC neurons (V1: $n = 50$ cells; SC: $n = 56$ cells; $p = 0.0049$ for dark condition between SC and V1 and $p = 6.35e\text{-}4$ for gray condition, KS test). For plots in ***G*** and ***H***, individual data points are overlaid on the box-whisker plots, which show the 25th, median, and 75th percentiles of the distributions.

It is important to note that the sSGS is a direct retinal target, whereas V1 layer 2/3 are farther away from the retina. The difference we revealed here could thus reflect their different positions along each visual pathway, rather than a difference between the two pathways. Indeed, studies of the mouse dLGN have reported various degrees of locomotion-dependent modulation (Niell and Stryker, 2010; Erisken et al., 2014; Aydın et al., 2018), but they are weaker than the modulation in V1. In fact, even the modulation of layer 4 neurons is weaker than that of layer 2/3 (Hoy and Niell, 2015; Dadarlat and Stryker, 2017), supporting the idea that state-dependent modulation might emerge later in visual pathways. V1 layer 5 neurons, which innervate SGS neurons through the cortico-collicular projection, also increase their visual responses during locomotion, even though their modulation is smaller compared with layer 2/3 neurons (Hoy and Niell, 2015; Dadarlat and Stryker, 2017). Whether and how layer 5 inputs modulate SGS response during locomotion remains unknown, as well as their cell-type-specific targeting. However, it is known that their axons display a depth-dependent profile in the SC (Wang and Burkhalter, 2013) and they can increase SGS response magnitude (Zhao et al., 2014). Together, all these considerations argue that it is possible that locomotion-dependent modulation could occur

in the lower SGS and deeper layers of the SC. A recent study using multielectrode recording, which severely under-sample sSGS neurons, has indeed reported diverse patterns of modulation in the SC (Ito et al., 2017), presumably mostly below the sSGS. Future studies will be needed to determine the depth-specific profile of such modulation in the SC, especially regarding certain cell types. Of particular interest are the wide-field vertical cells that are located at the bottom of the SGS (Gale and Murphy, 2016). With extremely broad dendrites, these cells integrate inputs from the retina, visual cortex, and local circuits, and send their outputs to the lateral posterior nucleus (the rodent pulvinar), which has been shown to carry locomotion signal to V1 (Roth et al., 2016). Such experiments will start to unravel how visual information that is faithfully encoded by the sSGS is further processed in the SC.

In our experiments, we imaged the caudal-medial pole of the SC, which corresponds to the dorsal-lateral part of the visual field. It thus remains possible that the sSGS neurons in other parts of the SC could be modulated by locomotion. This is an intriguing possibility considering the recent reports that stimulus orientation and direction may not be evenly represented by the SGS at all visual field locations (Ahmadlou and Heimel, 2015; Feinberg and Meister, 2015; de Malmazet et al., 2018). However, it is important to note that we have not seen such an organization in the sSGS (Inayat et al., 2015), and preferred directions distribute over the full range in the current dataset (Fig. 2*F*). These observations are again consistent with the notion that sSGS neurons encode visual scenes faithfully with an unbiased representation.

We also examined whether the sSGS responses evoked by particular stimulus directions were modulated by locomotion, and no obvious trend was seen. In other words, a posteriorly moving stimulus, which is in the direction of self-generated motion during locomotion, has a similarly small effect as the opposite stimulus. This was quite surprising considering the potential role of direction selectivity in encoding optic flow (Sabbah et al., 2017). However, in our experiments, the visual stimulus and the animal's locomotion was uncoupled. A "closed-loop" configuration such as in virtual reality (Keller et al., 2012; Zmarz and Keller, 2016) will be needed to determine the effect of optic flow on modulating direction selective responses. Nevertheless, we showed here that locomotion dramatically increases V1 responses under the exact same "open-loop" condition, thus highlighting important differences between V1 and the sSGS.

Response variability and spontaneous activity

Neuronal responses in the visual cortex are known to vary across trials (Churchland et al., 2010; Lin et al., 2015), meaning that the same visual input can generate different perceptual or behavioral outputs. Studies in V1 have also reported that locomotion decreases the Fano factor of spike count (Erisken et al., 2014) and the coefficient of variation of membrane potential responses (Bennett et al., 2013). We did not observe such a change in V1 during locomotion, presumably due to the inferior sensitivity of calcium imaging in quantifying response fidelity compared with physiological recordings. Despite this technical limitation, the difference in response variability is clear between the sSGS and V1. The more faithful encoding of visual motion by the sSGS is consistent with the role of the SC in the detection of threats, where reliable behavioral responses are crucial for the animal's survival.

Variability in neuronal responses has been suggested to depend on spontaneous activity (Arieli et al., 1996; Ferezou and Deneux, 2017). In V1, spontaneous activity is believed to contribute to the generation of prediction and to reflect the overall state of the network (Arieli et al., 1996). This type of non-sensory driven activity could allow greater flexibility in the evoked responses. In support of this idea, we found that the sSGS and V1 display different levels of spontaneous activity, which is consistent with their difference in response variability. The exact function of these differences in visual processing remains largely unknown. Future studies with more sophisticated behavioral design will be needed to examine how these two visual pathways, and their interactions, mediate our survival and perception.

References

Ahmadlou M, Heimel JA (2015) Preference for concentric orientations in the mouse superior colliculus. Nat Commun 6:6773.

Arieli A, Sterkin A, Grinvald A, Aertsen A (1996) Dynamics of ongoing activity: explanation of the large variability in evoked cortical responses. Science 273:1868–1871.

Ayaz A, Saleem AB, Schölvinck ML, Carandini M (2013) Locomotion controls spatial integration in mouse visual cortex. Curr Biol 23:890–894.

Aydın Ç, Couto J, Giugliano M, Farrow K, Bonin V (2018) Locomotion modulates specific functional cell types in the mouse visual thalamus. Nat Commun 9:4882.

Barchini J, Shi X, Chen H, Cang J (2018) Bidirectional encoding of motion contrast in the mouse superior colliculus. eLife 7:e35261.

Bennett C, Arroyo S, Hestrin S (2013) Subthreshold mechanisms underlying state-dependent modulation of visual responses. Neuron 80:350–357.

Brainard DH (1997) The psychophysics toolbox. Spat Vis 10:433–436.

Busse L, Cardin JA, Chiappe ME, Halassa MM, McGinley MJ, Yamashita T, Saleem AB (2017) Sensation during active behaviors. J Neurosci 37:10826–10834.

Cang J, Feldheim DA (2013) Developmental mechanisms of topographic map formation and alignment. Annu Rev Neurosci 36:51–77.

Cang J, Savier E, Barchini J, Liu X (2018) Visual function, organization, and development of the mouse superior colliculus. Annu Rev Vis Sci 4:239–262.

Chen TW, Wardill TJ, Sun Y, Pulver SR, Renninger SL, Baohan A, Schreiter ER, Kerr RA, Orger MB, Jayaraman V, Looger LL, Svoboda K, Kim DS (2013) Ultrasensitive fluorescent proteins for imaging neuronal activity. Nature 499:295–300.

Churchland MM, Yu BM, Cunningham JP, Sugrue LP, Cohen MR, Corrado GS, Newsome WT, Clark AM, Hosseini P, Scott BB, Bradley DC, Smith MA, Kohn A, Movshon JA, Armstrong KM, Moore T, Chang SW, Snyder LH, Lisberger SG, Priebe NJ, et al. (2010) Stimulus onset quenches neural variability: a widespread cortical phenomenon. Nat Neurosci 13:369–378.

Dadarlat MC, Stryker MP (2017) Locomotion enhances neural encoding of visual stimuli in mouse V1. J Neurosci 37:3764–3775.

De Franceschi G, Solomon SG (2018) Visual response properties of neurons in the superficial layers of the superior colliculus of awake mouse. J Physiol 596:6307–6332.

de Malmazet D, Kühn NK, Farrow K (2018) Retinotopic separation of nasal and temporal motion selectivity in the mouse superior colliculus. Curr Biol 28:2961–2969.e4.

Dipoppa M, Ranson A, Krumin M, Pachitariu M, Carandini M, Harris KD (2018) Vision and locomotion shape the interactions between neuron types in mouse visual cortex. Neuron 98:602–615.e8.

Ellis EM, Gauvain G, Sivyer B, Murphy GJ (2016) Shared and distinct retinal input to the mouse superior colliculus and dorsal lateral geniculate nucleus. J Neurophysiol 116:602–610.

Erisken S, Vaiceliunaite A, Jurjut O, Fiorini M, Katzner S, Busse L (2014) Effects of locomotion extend throughout the mouse early visual system. Curr Biol 24:2899–2907.

Feinberg EH, Meister M (2015) Orientation columns in the mouse superior colliculus. Nature 519:229–232.

Ferezou I, Deneux T (2017) Review: how do spontaneous and sensory-evoked activities interact? Neurophotonics 4:031221.

Fu Y, Tucciarone JM, Espinosa JS, Sheng N, Darcy DP, Nicoll RA, Huang ZJ, Stryker MP (2014) A cortical circuit for gain control by behavioral state. Cell 156:1139–1152.

Gale SD, Murphy GJ (2014) Distinct representation and distribution of vi-

sual information by specific cell types in mouse superficial superior colliculus. J Neurosci 34:13458–13471.
Gale SD, Murphy GJ (2016) Active dendritic properties and local inhibitory input enable selectivity for object motion in mouse superior colliculus neurons. J Neurosci 36:9111–9123.
Hoy JL, Niell CM (2015) Layer-specific refinement of visual cortex function after eye opening in the awake mouse. J Neurosci 35:3370–3383.
Hubel DH, Wiesel TN (1962) Receptive fields, binocular interaction and functional architecture in the cat's visual cortex. J Physiol 160:106–154.
Ibrahim LA, Mesik L, Ji XY, Fang Q, Li HF, Li YT, Zingg B, Zhang LI, Tao HW (2016) Cross-modality sharpening of visual cortical processing through layer-1-mediated inhibition and disinhibition. Neuron 89:1031–1045.
Inayat S, Barchini J, Chen H, Feng L, Liu X, Cang J (2015) Neurons in the most superficial lamina of the mouse superior colliculus are highly selective for stimulus direction. J Neurosci 35:7992–8003.
Ito S, Feldheim DA, Litke AM (2017) Segregation of visual response properties in the mouse superior colliculus and their modulation during locomotion. J Neurosci 37:8428–8443.
Iurilli G, Ghezzi D, Olcese U, Lassi G, Nazzaro C, Tonini R, Tucci V, Benfenati F, Medini P (2012) Sound-driven synaptic inhibition in primary visual cortex. Neuron 73:814–828.
Kara P, Reinagel P, Reid RC (2000) Low response variability in simultaneously recorded retinal, thalamic, and cortical neurons. Neuron 27:635–646.
Keller GB, Bonhoeffer T, Hübener M (2012) Sensorimotor mismatch signals in primary visual cortex of the behaving mouse. Neuron 74:809–815.
Kuffler SW (1953) Discharge patterns and functional organization of mammalian retina. J Neurophysiol 16:37–68.
Lee AM, Hoy JL, Bonci A, Wilbrecht L, Stryker MP, Niell CM (2014) Identification of a brainstem circuit regulating visual cortical state in parallel with locomotion. Neuron 83:455–466.
Levine JN, Chen H, Gu Y, Cang J (2017) Environmental enrichment rescues binocular matching of orientation preference in the mouse visual cortex. J Neurosci 37:5822–5833.
Liang F, Xiong XR, Zingg B, Ji XY, Zhang LI, Tao HW (2015) Sensory cortical control of a visually induced arrest behavior via corticotectal projections. Neuron 86:755–767.
Lin IC, Okun M, Carandini M, Harris KD (2015) The nature of shared cortical variability. Neuron 87:644–656.
Livingstone MS, Hubel DH (1981) Effects of sleep and arousal on the processing of visual information in the cat. Nature 291:554–561.
Maunsell JHR (2015) Neuronal mechanisms of visual attention. Annu Rev Vis Sci 1:373–391.
May PJ (2006) The mammalian superior colliculus: laminar structure and connections. Prog Brain Res 151:321–378.
Mineault PJ, Tring E, Trachtenberg JT, Ringach DL (2016) Enhanced spatial resolution during locomotion and heightened attention in mouse primary visual cortex. J Neurosci 36:6382–6392.
Niell CM, Stryker MP (2008) Highly selective receptive fields in mouse visual cortex. J Neurosci 28:7520–7536.
Niell CM, Stryker MP (2010) Modulation of visual responses by behavioral state in mouse visual cortex. Neuron 65:472–479.
Pakan JM, Lowe SC, Dylda E, Keemink SW, Currie SP, Coutts CA, Rochefort NL (2016) Behavioral-state modulation of inhibition is context-dependent and cell type specific in mouse visual cortex. eLife 5:e14985.
Polack PO, Friedman J, Golshani P (2013) Cellular mechanisms of brain state-dependent gain modulation in visual cortex. Nat Neurosci 16:1331–1339.
Poort J, Khan AG, Pachitariu M, Nemri A, Orsolic I, Krupic J, Bauza M, Sahani M, Keller GB, Mrsic-Flogel TD, Hofer SB (2015) Learning enhances sensory and multiple non-sensory representations in primary visual cortex. Neuron 86:1478–1490.
Reimer J, Froudarakis E, Cadwell CR, Yatsenko D, Denfield GH, Tolias AS (2014) Pupil fluctuations track fast switching of cortical states during quiet wakefulness. Neuron 84:355–362.
Roth MM, Dahmen JC, Muir DR, Imhof F, Martini FJ, Hofer SB (2016) Thalamic nuclei convey diverse contextual information to layer 1 of visual cortex. Nat Neurosci 19:299–307.
Sabbah S, Gemmer JA, Bhatia-Lin A, Manoff G, Castro G, Siegel JK, Jeffery N, Berson DM (2017) A retinal code for motion along the gravitational and body axes. Nature 546:492–497.
Saleem AB, Ayaz A, Jeffery KJ, Harris KD, Carandini M (2013) Integration of visual motion and locomotion in mouse visual cortex. Nat Neurosci 16:1864–1869.
Sarnaik R, Chen H, Liu X, Cang J (2014) Genetic disruption of the on visual pathway affects cortical orientation selectivity and contrast sensitivity in mice. J Neurophysiol 111:2276–2286.
Shang C, Liu Z, Chen Z, Shi Y, Wang Q, Liu S, Li D, Cao P (2015) A parvalbumin-positive excitatory visual pathway to trigger fear responses in mice. Science 348:1472–1477.
Shi X, Barchini J, Ledesma HA, Koren D, Jin Y, Liu X, Wei W, Cang J (2017) Retinal origin of direction selectivity in the superior colliculus. Nat Neurosci 20:550–558.
Shuler MG, Bear MF (2006) Reward timing in the primary visual cortex. Science 311:1606–1609.
Steriade M, Timofeev I, Grenier F (2001) Natural waking and sleep states: a view from inside neocortical neurons. J Neurophysiol 85:1969–1985.
Vinck M, Batista-Brito R, Knoblich U, Cardin JA (2015) Arousal and locomotion make distinct contributions to cortical activity patterns and visual encoding. Neuron 86:740–754.
Wang L, Sarnaik R, Rangarajan K, Liu X, Cang J (2010) Visual receptive field properties of neurons in the superficial superior colliculus of the mouse. J Neurosci 30:16573–16584.
Wang Q, Burkhalter A (2013) Stream-related preferences of inputs to the superior colliculus from areas of dorsal and ventral streams of mouse visual cortex. J Neurosci 33:1696–1705.
Wei P, Liu N, Zhang Z, Liu X, Tang Y, He X, Wu B, Zhou Z, Liu Y, Li J, Zhang Y, Zhou X, Xu L, Chen L, Bi G, Hu X, Xu F, Wang L (2015) Processing of visually evoked innate fear by a non-canonical thalamic pathway. Nat Commun 6:6756.
Whyland KL, Slusarczyk AS, Bickford ME (2019) GABAergic cell types in the superficial layers of the mouse superior colliculus. J Comp Neurol. Advance online publication. Retrieved August 9, 2019. doi:10.1002/cne.24754.
Zhao X, Liu M, Cang J (2014) Visual cortex modulates the magnitude but not the selectivity of looming-evoked responses in the superior colliculus of awake mice. Neuron 84:202–213.
Zingg B, Chou XL, Zhang ZG, Mesik L, Liang F, Tao HW, Zhang LI (2017) AAV-mediated anterograde transsynaptic tagging: mapping corticocollicular input-defined neural pathways for defense behaviors. Neuron 93:33–47.
Zmarz P, Keller GB (2016) Mismatch receptive fields in mouse visual cortex. Neuron 92:766–772.